A Comparative Study on the Mechatronic and Electronic Self-Powered Synchronized Switch Interfaces for Piezoelectric Energy Harvesting Systems

Haili Liu[a,b], Cong Ge[a], Junrui Liang[a,*] and Ya Wang[b]

[a]School of Information Science and Technology, ShanghaiTech University, Shanghai, China
[b]Mechanical Engineering, Stony Brook University, NY, USA

ABSTRACT

By scavenging the vibration energy from the ambience, the piezoelectric energy harvesting (PEH) technology provides one of the most promising solutions towards the everlasting power supplies for distributed wireless sensors. Given the capacitive characteristics of the piezoelectric devices, synchronized switch interface circuits, such as the synchronized switch harvesting on inductor (SSHI), have been developed towards the harvested power enhancement. The self-powered sensing, synchronization, and switching issues are essential for implementing these circuit innovations towards practical applications. This paper provides a comparative study on the recently proposed mechatronic self-powered SSHI (MSP-SSHI) and the existing electronic self-powered SSHI (ESP-SSHI) interfaces. The MSP-SSHI uses a single-pole-double-throw switch to simultaneously perform the sensing and switching functions. It reduces the switching threshold and energy losses caused by the semiconductors in the electronic solution, and also eliminates the high-voltage breakdown problem in MOS based ESP-SSHI. On the other hand, the distance between the pole and throws will introduce some switching phase difference under large vibrations. A piecewise linear model is built for analyzing the switching phase difference in MSP-SSHI. It was found that the damping ratio and stiffness of the mechanical switch can significantly influence the switching phase difference. Experimental result shows that the MSP-SSHI can effectively increase the harvested power under small and medium vibration levels, compared to the standard bridge rectifier; whereas, the ESP-SSHI performs better under medium and strong vibration.

Keywords: piezoelectric energy harvesting, synchronized switch interface circuits, self-powered SSHI, vibration sensor switch

1. INTRODUCTION

Piezoelectric energy harvesting (PEH) technology provides one of the most promising solutions for powering the distributed wireless sensor networks (WSNs) by scavenging the ambient vibration energy [1-4]. Piezoelectric structure and power conditioning circuits are two key parts for building an efficient energy harvesting system. In the studies of interface circuit, synchronized switch harvesting on inductor (SSHI) [5], and other synchronized switch interface circuits [6] can increase the energy harvesting capability by several hundred percent. In SSHI, we need to sense the maximum deforming instants of the piezoelectric transducer, and simultaneously turn on an inductive circuit branch for the charge stored in the piezoelectric element, such that the voltage across the piezoelectric element can be inverted after half of an RLC cycle. The voltage inversion at its extreme points can stop the energy return from electrical to mechanical parts [3] and thus enabling higher energy harvesting capability. The building blocks of series SSHI is shown in Figure 1. For the standalone application of SSHI, the *sensing*, *synchronization*, and *switching* functions should be self-contained without using any external sensor, power supply, and controller. Given this requirements, some electronic self-powered SSHI (EPS-SSHI) have been invented [7-9], which consists of three electronic functional blocks, i.e., voltage peak detector, comparator, and electronic switch. The functional blocks are usually realized by bipolar junction transistors (BJT) [7, 8] or metal oxide semiconductors (MOS) [9, 10], either of which introduce some side-effects [8, 11]. For example, in the BJT solutions, the open circuit voltage is decreased, and meanwhile a switching delay as well as a large threshold voltage are introduced [8]; in the MOS solutions, the workable peak voltage is confined by the rating voltage of the MOS processing, usually lower than 10 volt in existing studies [9, 10]. These side-effects discount the original improvement and confine the application of EPS-SSHI.

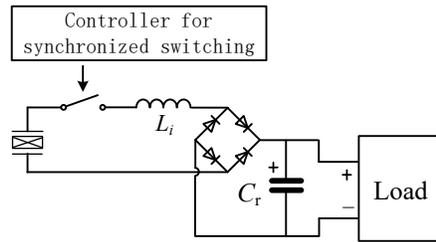* Corresponding author. Email: liangjr@shanghaitech.edu.cn

Figure 1. Diagram of a SSHI circuit

Aiming to overcome the aforementioned problems happened in the EPS-SSHI, some mechanical switch are studied to carry out the SSHI functions [11-13]. In these studies, the synchronized switches are realized by the mechanical contacts of a piezoelectric cantilever and two mechanical stoppers at each side of the cantilever. Yet, in their design, the vibration magnitude can be neither too small (cantilever cannot touch the stopper in small magnitude vibration) nor too large (strong collision might happen under large vibration). The stoppers confine the deflection of the cantilever, which makes this solution not very universal under variable vibration magnitude. Liu et al. [14] proposed another mechanical solution which attaches a low cost vibration sensor switch (VSS) at the free end of the piezoelectric cantilever. It was validated by experiments that the VSS can senses the maximum deflecting instants of a cantilever and automatically carries out synchronized switching actions. In the experiments, the VSS was realized by two single-wall VSSs and larger piezoelectric patch with heavier VSS mass and proof mass. Some phase lead occurred when applying larger excitation, and the phenomenon is left for future discussion. Later, Liu et al. [15] further developed a compact VSS which consists of a soft moving-beam pole and two rigid arc-shape throws. The arc-shape design can make the moving pole and the throws have a smoothly and firmly contact. Besides, the moving mass is placed out of the rigid frame, and thus can avoid collision with the frame. Based on this compact VSS, a mechatronic self-powered SSHI (MSP-SSHI) design is achieved. The mechanical VSS replaced the electronics used in the ESP-SSHI and meanwhile the circuit of the MSP-SSHI acts as a proof mass of the piezoelectric cantilever. In the previous study, experiments were conducted to compare its performance with a standard energy harvesting (SEH) circuit. While, the performance comparison between the MSP-SSHI and ESP-SSHI still needs to be further discussed.

This paper provides a comparative study on the MSP-SSHI and ESP-SSHI, in terms of harvested power under different vibration levels. Noting that voltage threshold and electronic losses of the ESP-SSHI usually maintain a constant level [16], the phase difference between the switching instant and the voltage extreme point may play key roles on the comparison between the MSP-SSHI and ESP-SSHI. Experiments on the switching phase difference of the two solutions are also conducted. A piecewise linear model is built for investigating the switching phase difference in MSP-SSHI.

2. ELECTRONIC SELF-POWERED SOLUTION

In PEH, a bridge rectifier and a filter capacitor (also acts as the energy storage) realize the simplest power conversion from ac to dc, therefore their combination is regarded as the standard energy harvesting (SEH) circuit. The SSHI technology improves the SEH by adding a switch and an inductive path into the SEH circuit. The switch synchronously turns on when the generated voltage reach its extreme points. To fulfill the functions of the SSHI circuit without using external power, the ESP-SSHI is realized by three electronic functional blocks, i.e., voltage peak detector, comparator, and electronic switch, as shown in Figure 2 (a). In the figure, the piezoelectric element is equivalent to three parallel-connected components, i.e. a current source, a clamped capacitor and an inherent resistor. From the topology of ESP-SSHI, the voltage threshold or voltage drop can be derived as follows [8]:

$$V_{thres} = V_{CE(\text{sat})} + 3V_D + V_{BE}, \tag{1}$$

where $V_{CE(\text{sat})}, V_D$ and V_{BE} are the collector-emitter saturation voltage, diode forward voltage drop and transistor base-emitter conducting voltage, respectively. The switching phase lag can also be calculated as follows

$$\phi = \cos^{-1}\left(1 - \frac{V_D + V_{BE}}{V_{OC}}\right) - \tan^{-1}\left[\frac{1}{\omega R_p (C_P + 2C_1)}\right], \tag{2}$$

where V_{OC} is the open circuit voltage across the piezoelectric element. Thus, the switching phase lag is not a constant value and will change with V_{OC}. The ESP-SSHI circuit discussed in this paper is realized by the BJT technology. The PCB is shown in Figure 2 (b). The electronic parts and parameters are the same as those in [8]. The threshold voltage V_{thres} is calculated to be 3.2 volt in this design. The switching phase lag changes when the piezoelectric element is excited under different vibration levels.
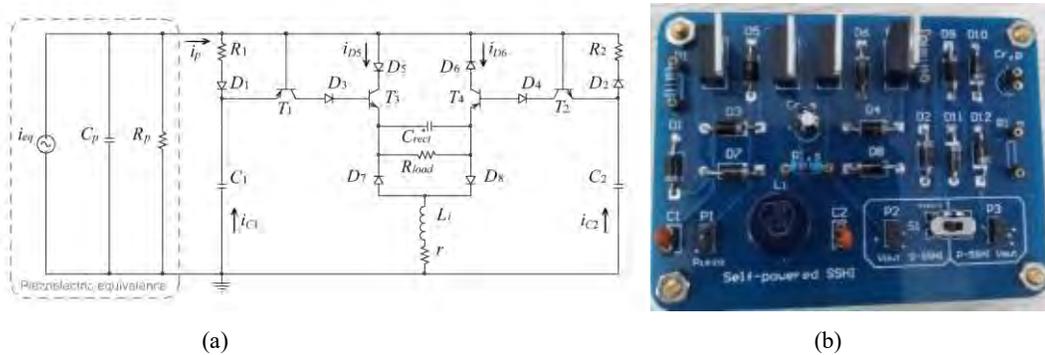

(a)   (b)

Figure 2. Electronic self-powered SSHI circuit. (a) Circuit topology [8]; (b) Printed circuit board (PCB) implementation.

3. MECHTRONIC SELF-POWERED SOLUTION

The working principle of the MSP-SSHI was introduced in [15], and the two switch instants are shown in Figure 3 (a). The experimental setup of the MSP-SSHI is shown in Figure 3 (b). Instead of using an arc-shape poles as [15] did, the rigid throws can be tuned with the adjustable screws. With this configuration, the influence of the distance between the moving pole and the throws on the switching phase difference can be investigated by tuning the screws; yet, the contact between the pole and the throws may go worse and collision problems may appear. The piezoelectric cantilever is made of a commercial piezoelectric bimorph (material: PZT-5H; d_{31}:-440pm/volt; model: QDTE52; manufacturer: Pant Piezoelectric Tech. Co., Ltd, Suzhou, China). One of the piezoelectric patch is used for energy harvesting purpose, while the other is used as the reference of beam deformation.
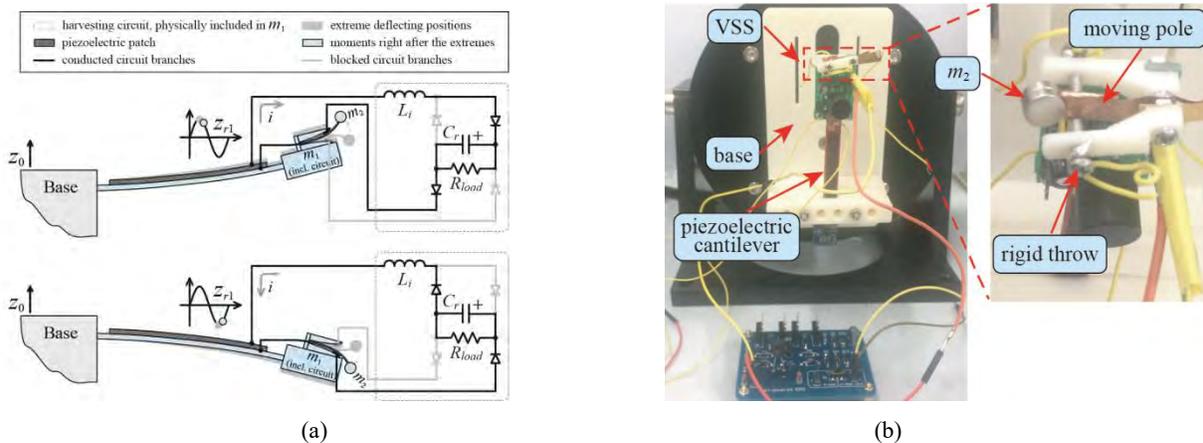

(a)   (b)

Figure 3.The mechanical self-powered SSHI. (a) Working principle [15]; (b) Experimental setup for the comparative study between the MSP-SSHI and ESP-SSHI.

4. COMPARATIVE STUDY

The ESP-SSHI and MSP-SSHI are experimentally compared, in terms of their output power under different excitation levels. In the comparison, the reference voltage is adjusted into the same value when testing different excitation levels. Figure 4(a) shows the optimum output power of the SEH, ESP-SSHI and MSP-SSHI at different open circuit voltage (reference voltage), which is proportional to excitation level. In the figure, the optimum output power is measured at the optimum load resistance of each interface circuit. Figure 4 (b) is an example for the optimum output power searching, where the reference voltage keeps at 20 volt in peak-to-peak value. From the Figure 4 (a), when the reference voltage is 6 volt, the ESP-SSHI can hardly output any power, this may cause by its threshold voltage. While, when exposed with strong excitation, the ESP-SSHI show its advantage over the MSP-SSHI. The ESP-SSHI outputs more power than MSP-SSHI when reference voltage is higher than 30 volt. The reason of the performance variation may lie in the switching phase difference variation. The performance of the MSP-SSHI and ESP-SSHI is also compared with that of the traditional SEH, and it is shown that the MSP-SSHI can output more power than SEH under larger range of excitation lever, and the advantage is more remarkable in lower excitation circumstance. On the contrary, the ESP-SSHI shows it advantage in higher excitation lever, while perform worse than SEH when exploring extreme weak excitations, e.g. the reference voltage is lower than 15 volt.

In general, MSP-SSHI outperforms SEH under small and medium vibration level; while ESP-SSHI outperforms SEH at medium and large vibration level.
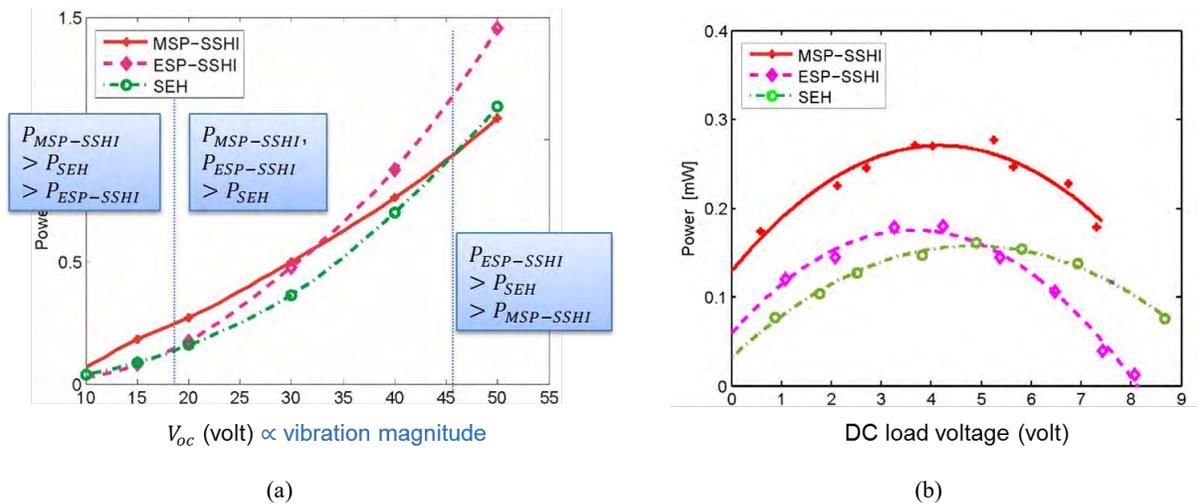

Figure 4. Power comparison of the SEH, ESP-SSHI, and MSP-SSHI at different vibration level. (a) Power comparison at different excitation level; (b) Example for optimum power point searching at the reference voltage of 20 volt.

Figure 5 (a) shows the waveforms of the ESP-SSHI and MSP-SSHI when the reference voltage keeps at 20 volt in peak-to-peak value. In the figure, the waveforms of the ESP-SSHI and the MSP-SSHI are recorded separately, and each time, one of them is recorded together with the reference voltage curves. Align the reference voltage curves measured at the two times, the phase relationship can be clearly shown in one figure. For SSHI, the ideal switch instants are at the extreme points of the reference voltage, as shown with the dashed line in Figure 5 (a). At this excitation level, the MSP-SSHI takes the switch action t_M ahead of the ideal instant, while the ESP-SSHI shows t_E delay. In Figure 5 (b), the switching phase difference of the ESP-SSHI and the MSP-SSHI at different reference voltage are compared. It can be observed from the figure that the switching phase difference of the ESP-SSHI decrease as the reference voltage increases, while the switching phase difference of the MSP-SSHI change from phase lag into phase lead, and then become greater than that of the ESP-SSHI in absolute value at higher reference voltage range. The phase lag of the ESP-SSHI is governed by (2), and thus will decrease as the open circuit voltage increases. The phase difference of the MSP-SSHI is mainly dominated by its dynamics, and will affect the performance of the MSP-SSHI. This may be the reason why ESP-SSHI outweighs MSP-SSHI in higher excitation level. Given the importance of the switching phase difference, it needs to be further discussed theoretically.

(a)

- **Low excitation level**
  $|\phi_{MSP}| < |\phi_{ESP}|$;

- **High excitation level**
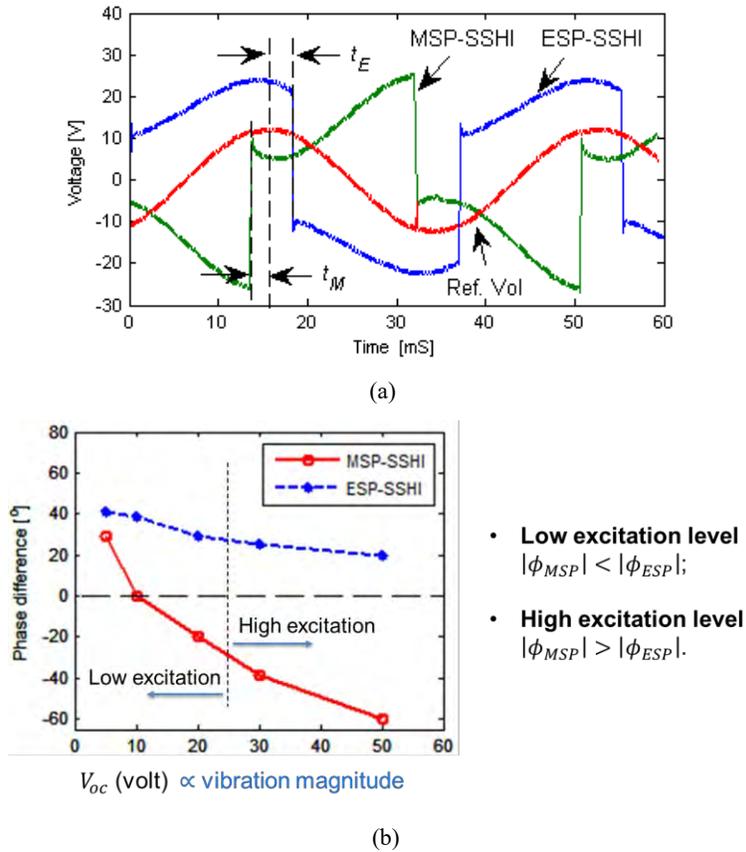 $|\phi_{MSP}| > |\phi_{ESP}|$.

(b)

Figure 5. Phase comparison of the ESP-SSHI and MSP-SSHI. (a) Waveforms of the two circuits at the reference voltage of 20 volt; (b) Phase comparison at different reference voltages (vibration levels).

5. DISCUSSION ON SWITCHING PHASE DIFFERENCE IN MECHANICAL SOLUTION

1.1 Modeling

In previous study [14, 15], the piezoelectric beam and the VSS were modeled as a linear two degree-of-freedom (2DOF) system, and an ideal waveform was assumed. In order to analysis the switching phase difference problem, a comprehensive model is built as shown in Figure 6. In the model, the mechanical part is represented as a piecewise-linear dynamic system: the piezoelectric cantilever is modeled as 1DOF, while the VSS will change its stiffness and damping ratio when the VSS beam reach the rigid throws at the two sides. The piezoelectric element is modeled as an idea transducer to study the electromechanical coupling effect, and a linear resistor is used to represent the load. In Figure 6., m_1, c_1, and k_1 are the equivalent mass, damping, and stiffness of the piezoelectric cantilever; m_2, c_2, and k_2 are the equivalent mass, damping and stiffness of the VSS when the VSS beam does not contact the rigid frame; c_3, and k_3 are the increased damping and stiffness of the VSS after the VSS beam contact the rigid frame; d is the equivalent distance between the equilibrium position of the VSS mass and the rigid throws; z_0 is the displacement of the vibrating base; z_1 and z_2 are the absolute displacements of m_1 and m_2, respectively; z_{r1} is the relative displacement of m_1 with respect to the base, and z_{r2} is that of m_2 with respect to m_1; α_p and C_p are the force-electricity factor and the clamped capacitor of the piezoelectric element; u is the voltage across the piezoelectric element; and Z_L is the equivalent load resistance.
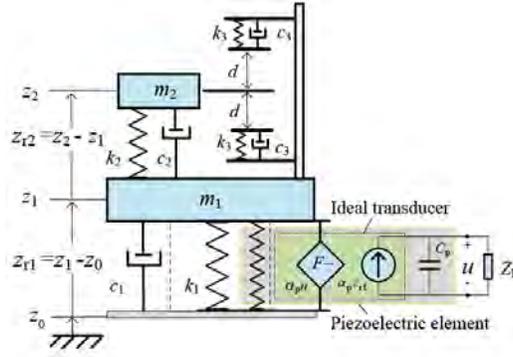
Figure 6. Piecewise-linear model of the MSP-SSHI.

In order to make the equations explicitly, we define the following parameters:

$$\bar{z}_{r1} = z_{r1}/d;\ \bar{z}_1 = z_1/d;\ \bar{z}_{r2} = z_{r2}/d;\ \tilde{m} = m_2/m_1;$$

$$\omega_j = \sqrt{k_j/m_j},\ \zeta_j = c_j/2m_j\omega_j,\ (j=1,2), \tag{3}$$

$$\omega_3 = \sqrt{k_3/m_2},\ \zeta_3 = c_3/2m_2\omega_3,$$

where $\tilde{m}$ is the mass ratio; ω_j is the angle resonant frequency; ζ_j is the damping ratio. Equation of motion of the VSS mass m_2, can be expressed as

$$\ddot{\bar{z}}_{r2} + (2\omega_2\zeta_2 + 2\omega_3\zeta_3)\dot{\bar{z}}_{r2} + (\omega_2^2 + \omega_3^2)\bar{z}_{r2} - \omega_3^2 = -\ddot{\bar{z}}_1 \qquad \bar{z}_{r2} > 1,$$

$$\ddot{\bar{z}}_{r2} + 2\omega_2\zeta_2\dot{\bar{z}}_{r2} + \omega_2^2\bar{z}_{r2} = -\ddot{\bar{z}}_1 \qquad\qquad -1 \le \bar{z}_{r2} \le 1, \tag{4}$$

$$\ddot{\bar{z}}_{r2} + (2\omega_2\zeta_2 + 2\omega_3\zeta_3)\dot{\bar{z}}_{r2} + (\omega_2^2 + \omega_3^2)\bar{z}_{r2} + \omega_3^2 = -\ddot{\bar{z}}_1 \qquad \bar{z}_{r2} < -1.$$

Equation of motion of m_1, can be written as

$$\ddot{\bar{z}}_{r1} + 2\omega_1\zeta_1\dot{\bar{z}}_{r1} + \omega_1^2\bar{z}_{r1} - \tilde{m}\left[(2\omega_2\zeta_2 + 2\omega_3\zeta_3)\dot{\bar{z}}_{r2} + (\omega_2^2 + \omega_3^2)\bar{z}_{r2}\right] + \tilde{m}\omega_3^2 + \frac{\alpha_p}{m_1}\bar{u} = -\ddot{\bar{z}}_0 \qquad \bar{z}_{r2} > 1$$

$$\ddot{\bar{z}}_{r1} + 2\omega_1\zeta_1\dot{\bar{z}}_{r1} + \omega_1^2\bar{z}_{r1} - \tilde{m}\left[2\omega_2\zeta_2\dot{\bar{z}}_{r2} + \omega_2^2\bar{z}_{r2}\right] + \frac{\alpha_p}{m_1}\bar{u} = -\ddot{\bar{z}}_0 \qquad\qquad -1 \le \bar{z}_{r1} \le 1 \tag{5}$$

$$\ddot{\bar{z}}_{r1} + 2\omega_1\zeta_1\dot{\bar{z}}_{r1} + \omega_1^2\bar{z}_{r1} - \tilde{m}\left[(2\omega_2\zeta_2 + 2\omega_3\zeta_3)\dot{\bar{z}}_{r2} + (\omega_2^2 + \omega_3^2)\bar{z}_{r2}\right] - \tilde{m}\omega_3^2 + \frac{\alpha_p}{m_1}\bar{u} = -\ddot{\bar{z}}_0 \qquad \bar{z}_{r1} < -1.$$

Circuit equation is

$$u/Z_L = \alpha_p\dot{z}_{r1} - C_p\dot{u}. \tag{6}$$

Rewrite equations (4) and (5) into 1-order derivative equation, and then the equations can be numerically solved by using the 4-order Runge-Kutta method. Taking equation (4) as an example, by defining intermediate variables $y_2 = \dot{\bar{z}}_{r2}, y_1 = \dot{\bar{z}}_{r1}$, equation (4) can be rewritten as a set of 1-order derivation equation:

$$\dot{y}_2 = -\dot{y}_1 - \left(2\omega_2\zeta_2 + 2\omega_3\zeta_3\right)y_2 - \left(\omega_2^2 + \omega_3^2\right)\bar{z}_{r2} + \omega_3^2 \qquad \bar{z}_{r2} > 1$$

$$\dot{y}_2 = -\dot{y}_1 - 2\omega_2\zeta_2 y_2 - \omega_2^2 \bar{z}_{r2} \qquad -1 \leq \bar{z}_{r2} \leq 1 \qquad (7)$$

$$\dot{y}_2 = -\dot{y}_1 - \left(2\omega_2\zeta_2 + 2\omega_3\zeta_3\right)y_2 - \left(\omega_2^2 + \omega_3^2\right)\bar{z}_{r2} - \omega_3^2 \qquad \bar{z}_{r2} < -1$$

$$\dot{\bar{z}}_{r2} = y_2.$$

Equation (7) can be further rewritten in a matrix form, and then can be solved by substituting into the 4-order Runge-Kutta equations.

1.2 Simulation

In simulation, the lumped parameters of the piezoelectric cantilever can be derived by using the method of [17, 18], and the equivalent mass m_1 is 33.4 g; the equivalent stiffness k_1 is 1.66 kN/m. In order to derive more general conclusions, the VSS parameters are normalized by defining the frequency ratio as $g_2 = \omega_2/\omega_1$ and $g_3 = \omega_3/\omega_1$. From the design guidelines of [15], a set of parameters are selected and listed in Table 1. The load resistor is chosen to be 1 MΩ since the SSHI circuit is open in most of time. In the Runge-Kutta method, the time step adopts 10 us and the total time of 1.5 sec are computed to get a steady-state solution.

Table 1. Mechanical parameters.

Parameters	Value
C_p (nF)	60
α_p (N/V)	0.02
Z_L (MΩ)	1
d (mm)	0.1 (case 1), 0.03 (case 2)
m_2/m_1	0.1
ω_2/ω_1	0.1
ω_3/ω_1	0.2 (case 1); 3 (case 2)
ζ_1	0.02
ζ_2	0.02
ζ_3	0.02 (case 1); 1 (case 2)

Figure 7 shows the switch logic of the VSS, which is simulated by using the parameters given in Table 1 (case 1). In the figure, the squared solid line stays zero or nonzero, which indicates the VSS turns off or turn on, respectively; the two horizontal dot lines show the distance d. As the VSS moving pole reaches one of the rigid throws, i.e. z_{r2} reaches d, the switch will turn on. The solid line is vertically inverted along the x-axis in the figure, which can make it intersect with the output voltage v_o (indicated by a dashed line), and thus the switching phase difference can be easily figured out. From the figure, we can see that the switching phase difference is mainly phase lead, and the phase lead will be significantly influenced by changing the value of z_{r1}/d. Figure 7 (b) shows the relationship between the phase lead and the normalized value of z_{r1}/d, where the normalized z_{r1}/d takes the parameters used in Figure 7 (a) as the reference. By tuning d, the normalized z_{r1}/d is increased, which cause phase lead increasing greatly, as shown in Figure 7 (b). Since z_{r1} is proportional to the input excitation, larger d will be needed when undergoing strong excitation, while, on the other hand, larger d may disable the switch in weak excitation, because the moving pole may not be able to touch the rigid throws.
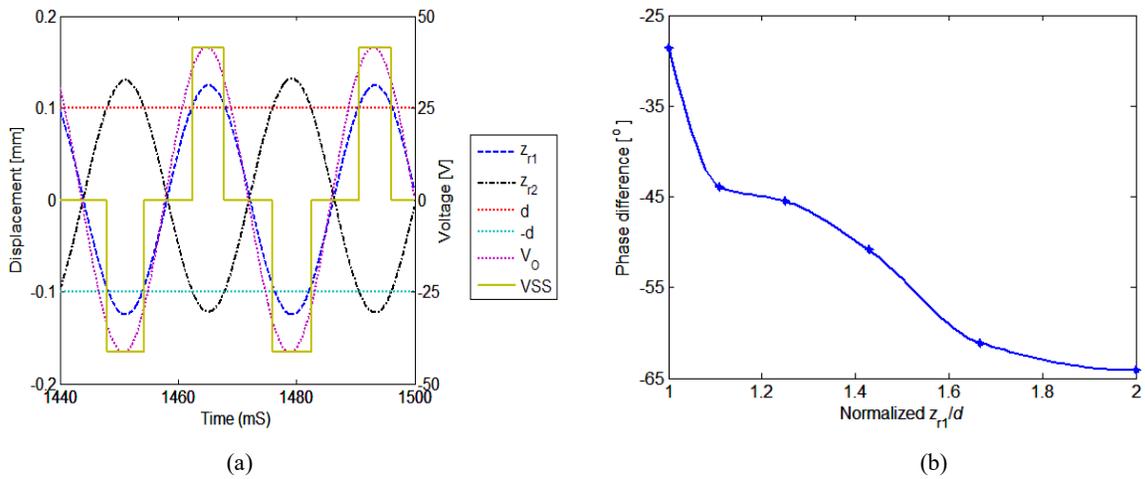
Figure 7. The switch logic of the MSP-SSHI and the switching phase difference variation with normalized z_{r1}/d. (a) the switch logic of the MSP-SSHI; (b) switching phase difference variation with normalized z_{r1}/d.

Through parameter study, it is found out that k_3 and ζ_3 can significantly affect the switching phase difference. Figure 8 (a) shows the switch logic, which is simulated by using the parameters in Table 1 (case 2). In this case, the VSS reaches the rigid throw d shortly after the extreme point, and then will move slowly and smoothly under the higher spring force and damping force. Since much smaller d is adopted, it will take few time to move from one rigid throw, e.g. d, to another rigid throw, e.g. $-d$. The switching phase difference is mainly determined by the distance d, and thus small d is preference in this situation. Figure 8 (b) shows that the switching phase difference change little with large normalized z_{r1}/d. In addition, studies show that larger ζ_3, say 3 or 5, can be used in larger normalized z_{r1}/d to decrease the switching phase difference.
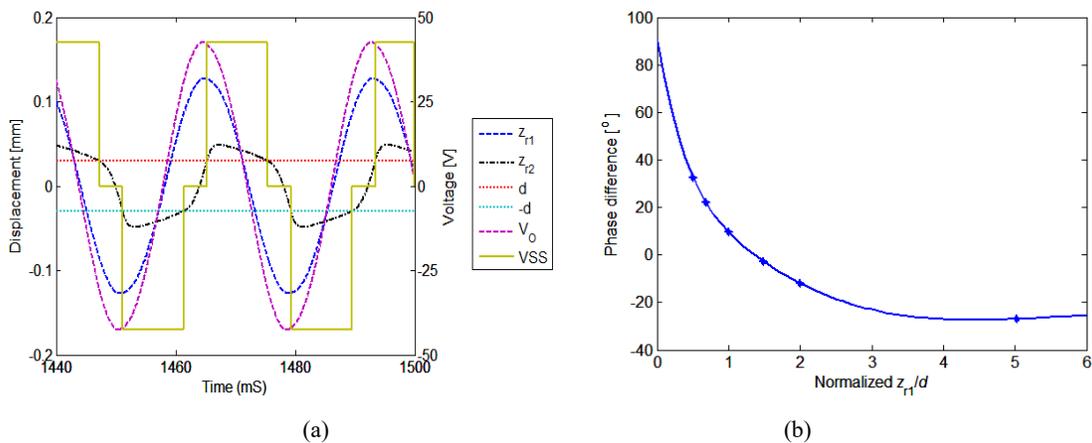

Figure 8. The switch logic and the switching phase difference variation when larger k_3 and ζ_3 are used ($g_3 = 3$, $\zeta_3 = 1$). (a) The switch logic of the MSP-SSHI; (b) Switching phase difference variation with normalized z_{r1}/d.

6. CONCLUSIONS

Comparative studies are conducted on the recently proposed MSP-SSHI and the exiting ESP-SSHI in terms of the output power at different vibration level. It is found that the MSP-SSHI can generate more power than the ESP-SSHI at weak excitations, while the ESP-SSHI outweigh the MSP-SSHI at strong excitations. The reason may lie in that the MSP-SSHI has no threshold and generates smaller switching phase difference at weak excitations, while its switching phase difference

becomes greater than that of the ESP-SSHI under strong excitation. An improved method which adopts larger damping and stiffness in the switch is discussed; simulations show that the damping ratio and stiffness largely affect the switching phase difference in MSP-SSHI. Further experimental validation and comprehensive evaluation are neened in our future works.

ACKNOWLEDGMENTS

REFERENCES

[1] S. R. Anton, and H. A. Sodano, "A review of power harvesting using piezoelectric materials (2003-2006)," Smart Materials and Structures, 16(3), R1-R21 (2007).

[2] J. Liang, and W. Liao, "Piezoelectric energy harvesting and dissipation on structural damping," Journal of Intelligent Material Systems and Structures, 20(5), 515-527 (2009).

[3] J. Liang, and W. Liao, "Energy flow in piezoelectric energy harvesting systems," Smart Materials and Structures, 20(1), 015005 (2011).

[4] R. L. Harne, and K. W. Wang, "A review of the recent research on vibration energy harvesting via bistable systems," Smart Materials and Structures, 22(2), (2013).

[5] D. Guyomar, A. Badel, E. Lefeuvre et al., "Toward energy harvesting using active materials and conversion improvement by nonlinear processing," IEEE Transactions on Ultrasonics Ferroelectrics and Frequency Control, 52(4), 584-595 (2005).

[6] D. Guyomar, and M. Lallart, "Recent Progress in Piezoelectric Conversion and Energy Harvesting Using Nonlinear Electronic Interfaces and Issues in Small Scale Implementation," Micromachines, 2(2), 274-294294 (2011).

[7] M. Lallart, and D. Guyomar, "An optimized self-powered switching circuit for non-linear energy harvesting with low voltage output," Smart Materials & Structures, 17(3), (2008).

[8] J. R. Liang, and W. H. Liao, "Improved Design and Analysis of Self-Powered Synchronized Switch Interface Circuit for Piezoelectric Energy Harvesting Systems," IEEE Transactions on Industrial Electronics, 59(4), 1950-1960 (2012).

[9] Y. Sun, N. H. Hieu, C.-J. Jeong et al., "An integrated high-performance active rectifier for piezoelectric vibration energy harvesting systems," Power Electronics, IEEE Transactions on, 27(2), 623-627 (2012).

[10] N. Krihely, and S. Ben-yaakov, "Self-contained resonant rectifier for piezoelectric sources under variable mechanical excitation," Power Electronics, IEEE Transactions on, 26(2), 612-621 (2011).

[11] F. Giusa, F. Maiorca, A. Noto et al., "A diode-less mechanical voltage multiplier: A novel transducer for vibration energy harvesting," Sensors and Actuators a-Physical, 212, 34-41 (2014).

[12] H. C. Liu, C. K. Lee, T. Kobayashi et al., "Investigation of a MEMS piezoelectric energy harvester system with a frequency-widened-bandwidth mechanism introduced by mechanical stoppers," Smart Materials and Structures, 21(3), (2012).

[13] Y. P. Wu, A. Badel, F. Formosa et al., "Nonlinear vibration energy harvesting device integrating mechanical stoppers used as synchronous mechanical switches," Journal of Intelligent Material Systems and Structures, 25(14), 1658-1663 (2014).

[14] H. Liu, C. Ge, and J. Liang, "A mechanical solution of self-powered SSHI interface for piezoelectric energy harvesting systems." 94311G-94311G-8.

[15] H. Liu, J. Liang, and C. Ge, "A mechatronic power boosting design for piezoelectric generators," Applied Physics Letters, 107(14), 141902 (2015).

[16] Y. S. Shih, S. C. Lin, M. Lallart et al., "Self-Powered Synchronized Switching Interfacing Circuits for Micro-Piezoelectric Energy Harvesters." 2.

[17] A. Badel, M. Lagache, D. Guyomar et al., "Finite element and simple lumped modeling for flexural nonlinear semi-passive damping," Journal of Intelligent Material Systems and Structures, 18(7), 727-742 (2007).

[18] H. Liu, T. Xu, Z. Huang et al., "Parametric design for a piezoelectric cantilever carrying oscillators to harvest multi-frequency vibration energy," International Journal of Applied Electromagnetics and Mechanics, 41(4), 389-405 (2013).